

# Formation of a Matter-Wave Bright Soliton

L. Khaykovich<sup>1</sup>, F. Schreck<sup>1</sup>, G. Ferrari<sup>1,2</sup>, T. Bourdel<sup>1</sup>  
J. Cubizolles<sup>1</sup>, L. D. Carr<sup>1</sup>, Y. Castin<sup>1</sup>, and C. Salomon<sup>1</sup>

<sup>1</sup>Laboratoire Kastler Brossel, Ecole Normale Supérieure,  
24 rue Lhomond, 75231 Paris CEDEX 05, France

<sup>2</sup>LENS-INFN, Largo E. Fermi 2, Firenze 50125, Italy

## Abstract

We report the production of matter-wave solitons in an ultra-cold  $^7\text{Li}$  gas. The effective interaction between atoms in a Bose-Einstein condensate is tuned with a Feshbach resonance from repulsive to attractive before release in a one-dimensional optical waveguide. Propagation of the soliton without dispersion over a macroscopic distance of 1.1 mm is observed. A simple theoretical model explains the stability region of the soliton. These matter-wave solitons open fascinating possibilities for future applications in coherent atom optics, atom interferometry and atom transport.

Solitons are localized waves that travel over long distances with neither attenuation nor change of shape as their dispersion is compensated by nonlinear effects. Soliton research has been conducted in fields as diverse as particle physics, molecular biology, geology, oceanography, astrophysics and nonlinear optics. Perhaps the most prominent application of solitons is in high rate telecommunications using optical fibers [1].

We use a Bose-Einstein condensate (BEC) of a dilute atomic gas of lithium atoms as a macroscopic matter-wave to form a soliton. Nonlinearity is provided by binary atomic interactions leading to the mean-field potential  $U(\vec{r}) = gn(\vec{r}) = 4\pi\hbar^2an(\vec{r})/m$ , where  $a$  is the scattering length,  $n(\vec{r})$  the spatial density and  $m$  the atomic mass. For  $a < 0$  the effective interaction is attractive and a trapped BEC is only stable for a number of atoms less than a critical number above which collapse occurs [2, 3, 4]. When the BEC is confined in only two directions, matter-waves have dispersion in the free direction due to their kinetic energy,  $E_{\text{kin}} \propto k^2$ , where  $k$  is the atomic wave vector. The balance between this dispersion and the attractive mean-field energy can lead to the formation of bright solitons as shown theoretically [5, 6, 7]. Up to now, only dark solitons have been observed in BEC's with repulsive interactions ( $a > 0$ ) [8, 9]. These solitons are characterized by a notch in the BEC density profile with a phase step across the soliton center. They propagate within the BEC with a velocity below the speed of sound, but so far are found to decay before reaching the edge of the condensate.

We report on the formation of a matter-wave bright soliton, a freely propagating self-bound atomic gas. The soliton is produced from a  ${}^7\text{Li}$  BEC in the internal atomic state  $|F = 1, m_F = 1\rangle$ . In this state a Feshbach resonance allows us to continuously tune the scattering length from a positive to negative value by means of an applied magnetic field [10, 11], a requirement for the production of a bright soliton.

In our experimental setup [12, 13, 14],  $4 \times 10^8$   ${}^7\text{Li}$  atoms are loaded from a magneto-optical trap into a strongly confining Ioffe-Pritchard (IP) magnetic trap. Atoms are in the  $|F =$

$2, m_F = 2\rangle$  state for which the scattering length is  $a = -1.4$  nm. Evaporative cooling lowers the temperature from 2 mK to 10  $\mu$ K after which  $\sim 6 \times 10^5$  atoms remain. Atoms are then transferred into a far detuned optical dipole trap at the intersection of two Nd:YAG gaussian laser beams (Fig. 1) with common waists of 38(3)  $\mu$ m [15]. The 9.5 W laser power is split between the two beams using two acousto-optic modulators.

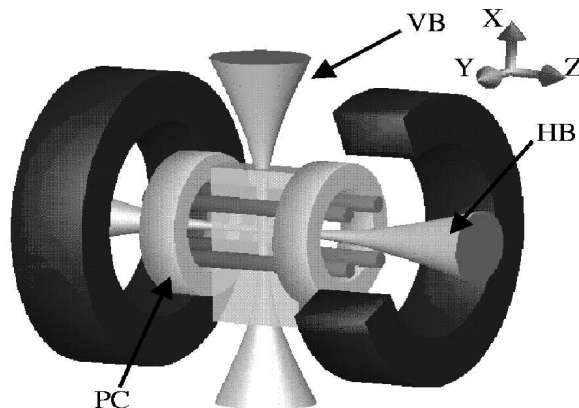


Figure 1: Experimental setup for soliton production.  ${}^7\text{Li}$  atoms are evaporatively cooled in a Ioffe-Pritchard magnetic trap and transferred into a crossed optical dipole trap in state  $|F = 1, m_F = 1\rangle$  where they Bose condense. Magnetic tuning of the scattering length to positive, zero and negative values is performed with the two pinch coils (PC). Switching-off the vertical trapping beam (VB) allows propagation of a soliton in the horizontal 1D waveguide (HB). Absorption images of solitons and BEC's are recorded on a CCD camera in the  $x, z$  plane.

The transfer from the magnetic trap to the optical trap is done in two steps. First, the power of the YAG beams is ramped over 200 ms to a value such that the radial oscillation frequency of the atoms is 1.8 kHz in the vertical beam and 3.3 kHz in the horizontal beam which matches that of the IP trap. Second, the magnetic trap is slowly turned off over 200 ms, keeping only a 5 G bias field. The transfer efficiency is nearly 100%. Then, transfer from the state  $|F = 2, m_F = 2\rangle$  to the state  $|F = 1, m_F = 1\rangle$  is performed by rapid adiabatic passage with a microwave frequency sweep scanning 1 MHz in 10 ms around 820 MHz. The transfer efficiency is better than 95%. Among all  ${}^7\text{Li}$  hyperfine states which can be trapped in

the dipole trap,  $|F = 1, m_F = 1\rangle$  is particularly useful as it is the lowest energy state in which 2-body losses, which are relatively strong in the state  $|F = 2, m_F = 2\rangle$  [13], are completely suppressed. Furthermore, this state is predicted to have a Feshbach resonance near 725 G [11], allowing magnetic tuning of the scattering length (Fig. 2). An adjustable magnetic field is produced by the pinch coils of our IP trap. Their inductance is small so that their current can be changed on a time scale shorter than  $\sim 200 \mu\text{s}$ . As in previous work on  $^{23}\text{Na}$  and  $^{85}\text{Rb}$  [16, 17], we locate the  $^7\text{Li}$  Feshbach resonance through observation of a dramatic loss of trapped atoms that we experimentally identify as due to 3-body recombination. The resonance position is found at 720(15) G, in good agreement with theory (725 G) [11].

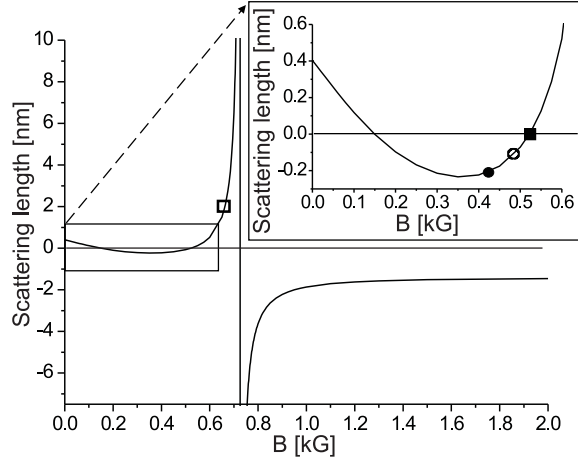


Figure 2: Predicted magnetic field dependence of the scattering length  $a$  for  $^7\text{Li}$  in state  $|F = 1, m_F = 1\rangle$  [11]. Inset: expanded view of the  $[0 - 0.6]$  kG interval with the various values of  $a$  used to study soliton formation. Open square: initial BEC. Square: Ideal BEC gas. Open circle: attractive gas. Dark circle: soliton.

We then produce a  $^7\text{Li}$  BEC in the crossed dipole trap by forced evaporation achieved by lowering the depth of the optical trapping potential [18]. Between  $B = 0$  and  $B = 590$  G the scattering length is small ( $|a| \leq 0.4$  nm), hindering efficient evaporative cooling (Fig. 2). Therefore, we operate at a magnetic field of 665 G in the wing of the Feshbach resonance where

$a \simeq +2.1$  nm and where 3-body losses remain moderate. The horizontal (vertical) optical power is lowered from 5.5 W (1.5 W) to 1.15 W (0.9 W) in 100 ms, and then to 0.27 W (0.19 W) in 150 ms. A condensate with  $N \sim 2 \times 10^4$  atoms, about half of the total number of atoms, is obtained in a nearly isotropic trap where atoms have oscillation frequencies of 710, 1000, 710 Hz along x, y, z. We then tune the scattering length to zero to reduce 3-body losses.

In order to transform the BEC into a bright soliton, the trapping geometry is adiabatically deformed to a cylindrical geometry obtained by keeping only the horizontal trapping beam. To ensure adiabatic deformation of the condensate, the vertical beam power is ramped down to 3 mW in 200 ms, which reduces the axial oscillation frequency of the atoms to  $\omega_z \simeq 2\pi \times 50$  Hz while the radial oscillation frequency remains  $\omega_{\perp} = 2\pi \times 710$  Hz. The effective interaction is then tuned through changes in the magnetic field in 50 ms. Finally, switching off the vertical beam with a mechanical shutter releases the BEC into the horizontal 1D waveguide. In the axial direction the coils that are used to provide the offset field produce a slightly expulsive harmonic potential for the state  $|F = 1, m_F = 1\rangle$  which overcomes the dipole trap. The resulting axial force on the atoms is conveniently written as  $-m\omega_z^2 z$  where the frequency  $\omega_z$  is now imaginary. Typically  $\omega_z = 2i\pi \times 78$  Hz for  $B = 520$  G. After an adjustable evolution time in the horizontal guide, the bias magnetic field is turned off and 400  $\mu$ s later an absorption image is recorded (Fig. 3) where the formation of the soliton is seen.

We compare the evolution of an ideal gas (Fig. 3A)),  $a \simeq 0$  for  $B=520$  G, with a gas with attractive interactions (Fig. 3B,SFig. 3B),  $a = -0.21$  nm for  $B = 425$  G. In both cases the cloud drifts towards the left because of a small offset,  $\simeq 50 \mu$ m, between the maximum of the expulsive potential and the initial position of the atoms. The width of the expanding cloud in the horizontal waveguide is considerably broader in the non-interacting case, while for all times of observation the soliton width remains equal to the resolution limit of our imaging system,  $9(1) \mu$ m axially [19]. The cloud contains  $6(2) \times 10^3$  atoms and propagates over a distance of

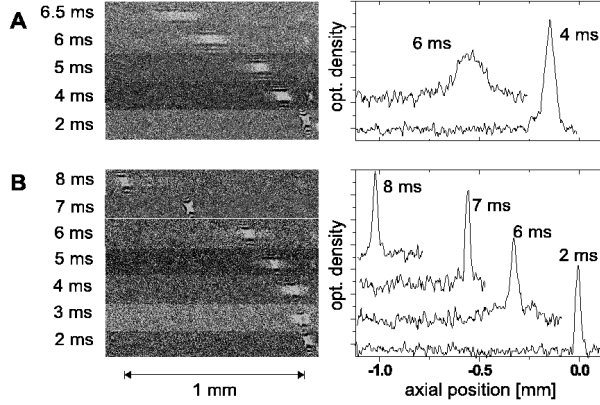


Figure 3: Absorption images at variable delays after switching off the vertical trapping beam. Propagation of an ideal BEC gas (A) and of a soliton (B) in the horizontal 1D waveguide in presence of an expulsive potential. Propagation without dispersion over 1.1 mm is a clear signature of a soliton. Corresponding axial profiles integrated over the vertical direction.

1.1 mm without any detectable dispersion, a clear signature of a bright soliton [20]. No decay of the soliton is observed in the 10 ms it remains in the detection region. A substantial fraction of atoms,  $\simeq 2/3$ , remains in a non-condensed pedestal around the soliton, clearly visible for intermediate propagation times in the guide.

We then made measurements of the wave-packet size versus propagation time for three values of the scattering length:  $a \simeq 0$ ,  $a \simeq -0.11$  nm and  $a \simeq -0.21$  nm (Fig. 4). For  $a \simeq 0$  (Fig. 4A), the interaction between atoms is negligible and the size of the cloud is governed by the expansion of the initial condensate distribution under the influence of the negative curvature of the axial potential. The measured size is in excellent agreement with the predicted size of a non-interacting gas subjected to an expulsive harmonic potential: taking the curvature as a fit parameter (solid line in Fig. 4A), we find  $\omega_z = 2i\pi \times 78(3)$  Hz, which agrees with the expected value of the curvature produced by the pinch coils [14]. For  $a = -0.11$  nm and  $B = 487$  G the size of the wave-packet is consistently below that of a non-interacting gas (Fig. 4B : solid line). Attractive interactions reduce the size of the atomic cloud but are not strong enough to

stabilize the soliton against the expulsive potential. When  $a$  is further decreased to  $-0.21$  nm the measured size of the wave packet no longer changes as a function of guiding time, indicating propagation without dispersion even in presence of the expulsive potential (Fig. 4C).

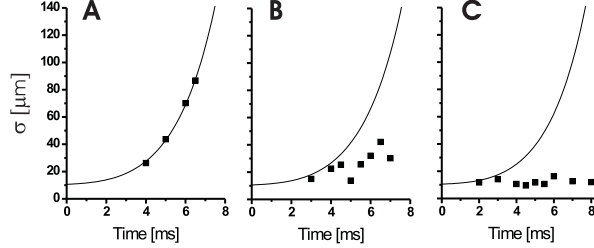


Figure 4: Measured r.m.s size of the atomic wave-packet Gaussian fit as a function of propagation time in the waveguide. (A):  $a = 0$ , ideal gas case; (B):  $a = -0.11$  nm; (C):  $a = -0.21$  nm; solid lines: calculated expansion of a non-interacting gas in the expulsive potential.

To theoretically analyze the stability of the soliton, we introduce the three-dimensional Gross-Pitaevskii energy functional

$$E_{\text{GP}} = \int d^3r \frac{\hbar^2}{2m} |\nabla \Psi(\vec{r})|^2 + \frac{Ng}{2} |\Psi(\vec{r})|^4 + \frac{1}{2}m [\omega_{\perp}^2 (x^2 + y^2) + \omega_z^2 z^2] |\Psi(\vec{r})|^2, \quad (1)$$

where the condensate wave-function  $\Psi$  is normalized to one. In Eq. 1 the first term is the kinetic energy responsible for dispersion, the second term is the interaction energy, which in the present case of attractive effective interactions ( $g < 0$ ) causes the wave-function to sharpen, and the third term is the external potential energy. We introduce the following two-parameter variational ansatz to estimate minimal energy states of  $E_{\text{GP}}$ :

$$\Psi(\vec{r}) = \frac{1}{\sqrt{2\pi\sigma_{\perp}^2 l_z}} \frac{1}{\cosh(z/l_z)} \exp\left(-\frac{x^2 + y^2}{2\sigma_{\perp}^2}\right), \quad (2)$$

where  $\sigma_{\perp}$  and  $l_z$  are the radial and axial widths of the wave-function. The functional form of the well-known 1D soliton has been chosen for the longitudinal direction [5], while in the

transverse direction a Gaussian ansatz is the optimal one for harmonic confinement. For each  $l_z$  we minimize the mean energy over  $\sigma_\perp$ ; the resulting function of  $l_z$  is plotted (Fig. 5) for various values of the parameter  $Na/a_\perp^{\text{ho}}$  where  $a_\perp^{\text{ho}} = (\hbar/m\omega_\perp)^{1/2}$ . For very small axial sizes, the interaction energy becomes on the order of  $-\hbar\omega_\perp$  and the gas loses its quasi-1D nature and collapses [3, 4]. For very large axial sizes the expulsive potential energy dominates and pulls the wave function apart. For intermediate sizes, attractive interactions balance both the dispersion and the effect of the expulsive potential; the energy presents a local minimum (solid line in Fig. 5). This minimum supports a macroscopic quantum bound state. However, it exists only within a narrow window of the parameter  $Na/a_\perp^{\text{ho}}$ . In our experiments  $\omega_\perp = 2\pi \times 710$  Hz and  $\omega_z = 2i\pi \times 70$  Hz for  $B = 420$  G, so that  $a_\perp^{\text{ho}} = 1.4 \mu\text{m}$ ; for  $N|a|$  larger than  $(N|a|)_c = 1.105 \mu\text{m}$ , a collapse occurs (dashed curve in Fig. 5), while for  $N|a|$  smaller than  $(N|a|)_e = 0.88 \mu\text{m}$  the expulsive potential causes the gas to explode axially (dotted curve in Fig. 5).

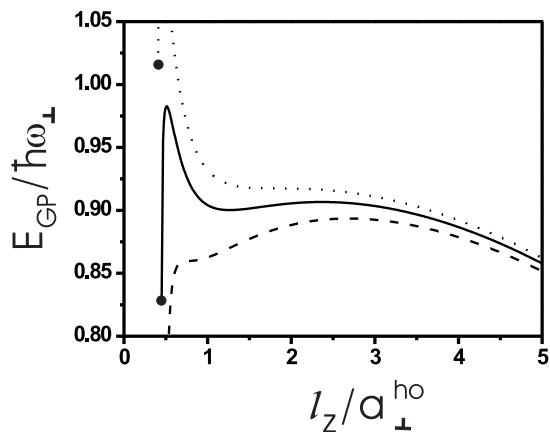


Figure 5: Theoretical energy diagram of an attractive Bose gas subjected to an expulsive potential for  $\omega_z/\omega_\perp = i \times 70/710$ . The energy as a function of the axial size after minimization over the transverse size is shown for three values of  $N|a|$ : within the stability window (solid curve); at the critical point for explosion  $(N|a|)_e$  (dotted curve); and at the critical point for collapse  $(N|a|)_c$  (dashed curve). End points of the curves indicate collapse, i.e.  $\sigma_\perp = 0$ .



For our experimental conditions and  $a = -0.21$  nm, the number of atoms which allows the soliton to be formed is  $4.2 \times 10^3 \leq N \leq 5.2 \times 10^3$ , in good agreement with our measured number  $6(2) \times 10^3$ . The expected axial size of the soliton is  $l_z \simeq 1.7 \mu\text{m}$ , which is below the current resolution limit of our imaging system. To verify the presence of a critical value of  $(Na)_e$  needed to stabilize the soliton, we have performed the measurements with the same  $a$  but with a reduced number of atoms,  $N = 2 \times 10^3$ . At 8 ms guiding time the axial size of the wave packet increased to  $30 \mu\text{m}$  indicating that no soliton was formed.

One may speculate as to the formation dynamics of the soliton in the elongated trap before its release in the optical waveguide. As the atom number in the initial BEC,  $2 \times 10^4$ , is about three times larger than the measured atom number in the soliton, it is likely that during the 50 ms phase where  $a$  is changed from 0 to negative values one or several collapses occur until the critical number for a stable BEC is reached. Indeed, the collapse time constant is predicted to be much less than 50 ms for our experimental conditions [21]. During the transfer into the 1D waveguide the BEC is transformed into a soliton and the non-condensed cloud is clearly observed at guiding times up to 6 ms as a broader background distribution. Non-adiabatic projection of the BEC from the confining onto the expulsive potential is expected to play a negligible role here according to numerical simulations [22]. At longer times the non-condensed atoms spread apart and become undetectable. Thus during the propagation phase the soliton decouples itself from the non-condensed fraction, resulting in a nearly pure soliton.

Finally, removal of the expulsive axial potential will allow us to significantly extend the stability domain towards lower values of  $N|a|$  and longer observation times. The soliton size could then be measured in situ, as well as its lifetime. The study of coherence properties of solitons and of binary collisions between solitons are immediate extensions of the present work.

## References and Notes

- [1] See for example the recent special issue: *Chaos* **10**, 471 (2000).
- [2] P. A. Ruprecht, M. J. Holland, K. Burnett, M. Edwards, *Phys. Rev. A* **51**, 4704 (1995).
- [3] C. C. Bradley, C. A. Sackett, R. G. Hulet, *Phys. Rev. Lett.*, **78** 985 (1997).
- [4] J. L. Roberts, *et al. ibid.* **86**, 4211 (2001).
- [5] V. E. Zakharov, A. B. Shabat, *Sov. Phys. JETP* **34**, 62 (1972).
- [6] V. M. Pèrez-Garcìa, H. Michinel, H. Herrero, *Phys. Rev. A* **57**, 3837 (1998).
- [7] L. D. Carr, M. A. Leung, W.P. Reinhardt, *J. Phys. B* **33** , 3983. (2000).
- [8] S. Burger *et al.*, *Phys. Rev. Lett.* **83**, 5198 (1999).
- [9] J. Denschlag *et al.*, *Science* **287**, 97 (2000).
- [10] E. Tiesinga, B. J. Verhaar, H. T. S. Stoof, *Phys. Rev. A* **47**, 4114 (1993).
- [11] V. Venturi, C. Williams, private communication.
- [12] M.-O. Mewes, G. Ferrari, F. Schreck, A. Sinatra, C. Salomon, *Phys. Rev. A* **61**, 011403R (2000).
- [13] F. Schreck *et al.*, *Phys. Rev. A* **64**, 011402R (2001).
- [14] F. Schreck *et al.*, *Phys. Rev. Lett.*, **87** 080403 (2001).
- [15] See, for instance, R. Grimm, M. Weidemüller, Y. B. Ovchinnikov, *Adv. in At. Mol. Opt. Physics* **42**, 95 (2000).
- [16] S. Inouye *et al.*, *Nature* **392**, 151 (1998).

- [17] J. L. Roberts, N. R. Claussen, S. L. Cornish, C. E. Wieman, Phys. Rev. Lett., **85**, 728 (2000).
- [18] M. D. Barrett, J. A. Sauer, M. S. Chapman, Phys. Rev. Lett., **87**, 010404 (2001).
- [19] In the vertical direction, a residual astigmatism of the imaging system gives a resolution limit of  $16 \mu\text{m}$ .
- [20] Over this distance, the change in magnetic field due to the curvature is 0.1 G, therefore the change in the scattering length is negligible (Fig. 2).
- [21] Y. Kagan, A. E. Muryshev, G. V. Shlyapnikov, Phys. Rev. Lett., **81**, 933 (1998).
- [22] L. D. Carr, Y. Castin, submitted to Phys. Rev. A (2002).
23. We are grateful to K. Corwin, M. Olshanii, G. Shlyapnikov, C. Williams, V. Venturi and B. Esry for important contributions to this work and to J. Dalibard and C. Cohen-Tannoudji for useful discussions. F.S. was supported by the DAAD, G.F. by the EU network CT 2000-00165 CAUAC, and L.D.C. by the NSF mps-drf 0104447. This work was supported by CNRS, Collège de France and Région Ile de France. Laboratoire Kastler Brossel is *Unité de recherche de l'Ecole Normale Supérieure et de l'Université Pierre et Marie Curie, associée au CNRS*.